LAPIN AMK
Lapland University of Applied Sciences

FLUXGATE MAGNETOMETER CALIBRATION

Biot-Savart Calibration Method

Russell, Andrew

Thesis
Technology, Communication and Transport
Degree Programme in Information Technology (Rovaniemi)
Bachelor of Engineering

2017

LAPIN AMK
Lapland University of Applied Sciences

Abstract of Thesis

School of Technology, Communication and Transport
Degree Programme in Information Technology
Bachelor of Engineering

Author Andrew Russell Year 2017
Supervisors Jouko Teeriaho & Veikko Keränen
Commissioned by
Title of Thesis Fluxgate Magnetometer Calibration Method
Number of pages 38 + 2

The aim of the study was to investigate if the law of Biot-Savart could be applied to a method to calibrate a fluxgate magnetometer at Arctic latitudes. The fluxgate sensor to be calibrated was commercially produced and included integrated signal acquisition and output interface circuitry. A mu-metal alloy magnetic field shielding chamber was not available for this study. Standard laboratory test equipment and apparatus were utilized to produce a calibration method with a very modest budget.

The law of Biot-Savart was applied to a current loop with square geometry.
An equation was derived for the magnitude of the magnetic field at the center of the square current loop. The magnetic field produced was directly proportional to the current flowing through the current loop. The resulting magnetic field was produced in opposition to the ambient geomagnetic field. Taking real-time data from the geophysical observatory at Sodankylä provided an accurate reading for each component of the geomagnetic field. By cancelling the geomagnetic field, the output of the fluxgate sensor was obtained while the magnitude of the surrounding geomagnetic field had been reduced to zero. By varying the current through the square current loop, a range of output values against a range of magnetic field magnitudes were achieved, allowing the linearity of the fluxgate sensor to be observed.

Results for the method were achieved only in the z-axis since this is the strongest component of geomagnetic field at arctic latitudes. Results in the *x*-axis and *y*-axis were not achieved, being weaker and varied considerably with slight changes in orientation. The absence of a precision mechanism to hold the fluxgate sensor in geographic North-South and East-West alignment made measurements impracticable. The results achieved in the vertical *z*-axis were consistent and allowed the output of the fluxgate sensor to be plotted against magnetic flux density.

Key words: Biot-Savart, calibration, fluxgate, geomagnetism, magnetometer

CONTENTS

LIST OF FIGURES

1 INTRODUCTION

Children play with magnetic toys. The invisible force that pulls opposite poles together induces a response of surprise and near disbelief in their eyes. Looking to their parents for an explanation, we dismiss this profound question with a simple one word answer, magnetism.

The magnetic field of the earth has been studied for centuries and its origin remains one of academic debate. Transient fluctuations in the strength of the Earth's magnetic field were first observed in 1722 by George Graham, a London clockmaker. He observed the fluctuations of a compass needle under a microscope. The first scientist to measure the earth's magnetic field was Carl Friedrich Gauss in 1835. (Merrill, McElhinny & McFadden 1998, 13.)

In modern times, Einstein, shortly after writing his special relativity paper in 1905, described the problem of the origin of the Earth's magnetic field as being one of the most important unsolved problems in physics (Merrill, McElhinny & McFadden 1998, 17). Today scientists suggest that the Earth's molten iron rich outer core works as a dynamo. The electricaly conducting molten metal of the outer core, moving in the faint magnetic field of the sun, the resulting electric currents creating the Earth's magnetic field. (Merrill, McElhinny & McFadden 1998, 305-308.)

The magnetic field of the Earth is shaped by the solar wind, pushed closer on the sunlit side and extended on the dark side, it forms a tear drop shape. It deflects not only harmful radiation but also charged particles carried on the solar wind. The velocity and concentration of charged particles in the solar wind varies with solar activity. The path of these particles creates a magnetic field that interferes with that of the Earth. Thus by observing geomagnetic pulsations, scientists are able to study the behaviour of charged particles of the solar wind as they collide with the Earth's magnetosphere. From the study of geomagnetic pulsations, researches are observing the nature of the particles of the solar wind and of the plasma around the Earth. (McPherron 2004.)

The geomagnetic field of the Earth is created by the movement of molten iron rich outer core of the earth. Changes in outer core occur over hundreds of years, thus the magnetic field it creates is stable. The fluctuations in geomagnetic field that are recorded at geophysical observatories around the globe are not observing changes caused by fluctuations in the Earth´s outer core, but rather fluctuations in space weather, the stream of charged particles emitted by the sun. This stream of charged particles varies in strength with solar activity. During solar storms, solar flares and coronal mass ejections that are emitted into the path of the Earth cause large variations in geomagnetic field. (McPherron 2004.)

Magnetometers at geophysical observatories measure the geomagnetic field in three alignments, North, East and vertically down. These detailed observations are of interest to scientists studying changes in the earth´s magnetosphere. There are several different types of sensors used to measure geomagnetic field strength. In this study a fluxgate sensor will be used for reasons of budget and practicality.

The goal of this study is to investigate the practicability of using the law of Biot-Savart to calibrate a commercially manufactured fluxgate magnetometer sensor at Arctic latitude. Tests will be performed without the use of a magnetic field shielding chamber, thus the calibrating magnetic field required must be of sufficient magnetic flux density to cancel the ambient geomagnetic field in the axis of study. The fluxgate sensor will be aligned in the axis of study without the use of a precision alignment mechanism, all alignments will be made with simple desktop apparatus.

The study attempts to record the sensor output time period over the range of zero Tesla to full geomagnetic flux density. The output signal of the fluxgate sensor under calibration varies in frequency with the density of magnetic flux. The time period of the output signal is read from the screen of a digital oscilloscope. The most important variables under scrutiny are the geometry of the current loop, the number of turns in the current loop coil and the current that flows through it.

2 PURPOSE AND OBJECTIVE

This thesis is a study of the design of a calibration method that is applicable for a commercially manufactured fluxgate magnetometer sensor situated at Arctic latitude. The law of Biot-Savart was applied to a practical design, which used a square current loop to produce a predetermined magnetic field on the sensor under test. The geometry of the square current loop allowed the magnetic flux density at its center to be calculated based on the number of turns of wire in the current loop and the current that was passed through it. The square current loop was designed so that it could carry sufficient current to produce a magnetic field to completely oppose the geomagnetic field in the *z*-axis. At Arctic latitudes the *z*-axis, vertically down into the Earth, is the predominant component of the geomagnetic field.

The objective of the method was to observe the linearity of the fluxgate sensor under test. The current loop power supply was varied to produced a range of static magnetic flux densities. The laboratory used had no magnetic shielding therefore the sensor was calibrated in the ambient geomagnetic field. The fluxgate sensor was aligned in the *z*-axis of the geomagnetic field and the current loop magnetic field was produced in opposition to the *z*-axis component of the geomagnetic field. The power supply current was increased incrementally until the calibration field completely cancelled the geomagnetic field, thus calibrating the sensor output at zero magnetic flux density. From the range of results plotted, the linearity of the fluxgate magnetometer sensor was observed.

3 THEORETICAL BASIS

3.1 Magnetic Field Elements

The magnetic field of the Earth, which is also known as the geomagnetic field, may be expressed in two different forms, scalar and vector. The scalar measurement states simply how much magnetic field there is at a particular point, where as a vector measurement gives the field strength in three separate directions that are perpendicular to each other, *x* (North), *y* (East) and *z* (down). The addition of these three vectors results in a quantity that is the scalar value, or the intensity of the magnetic field. There are two more terms that are often used with geomagnetism, declination (D) and inclination (I). The angle between geographic North and magnetic North, referred to as declination. Inclination is measured facing magnetic North, the angle that the geomagnetic field makes below the horizon down into the Earth, also referred to as dip. (Merrill, McElhinny & McFadden 1998, 20.)

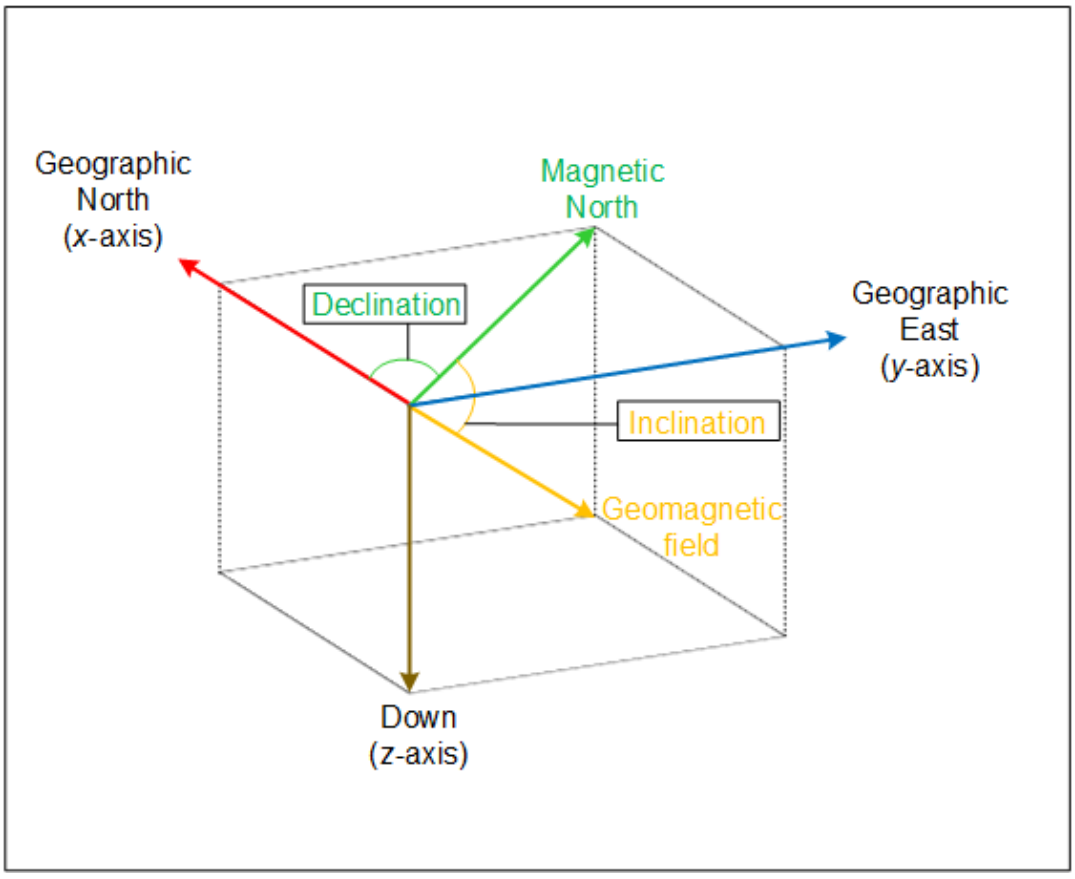

Figure 1. Geomagnetic Coordinate System

Direct measurements of the Earth´s magnetic field (usually quoted in the magnetic induction units of nanotesla) are made continuously at magnetic observatories, and are obtained from various oceanographic, land, aircraft and satellite surveys. Magnetic field may also be expressed in Gauss or Oersted and conversion between these units requires careful algebraic calculation. Magnetic field magnitude is notated by the letter H. Geomagnetism is often displayed with an isomagnetic chart, which is a contour map of the magnitude of the magnetic field. Other magnetic elements may also be illustrated with charts, isogonic chart charts are contour maps of the declination of magnetic field and isoclinic charts for inclination of magnetic field. (Merrill, McElhinny & McFadden 1998, 19-23.)

It is generally accepted in the scientific world that the source of the Earth´s magnetism is a result of the circulating flow of hot molten iron in the outer core of the earth acting as a giant dynamo. The outer core boundary with the mantle occurs at a depth of 2 891 km beneath the Earth´s crust (Merrill, McElhinny & McFadden 1998, 274.) Since the outer-core produces the geomagnetic field, this explains why the geomagnetic field inclination increases downwards at Arctic latitudes and upwards at Antarctic latitudes (Merrill, McElhinny & McFadden 1998, 23).

Any instrument used to measure geomagnetism requires vector values in three dimensions in order to give any context to the magnitude of the value. Thus an instrument to measure geomagnetism requires a tri-axial sensor aligned with geographic North, geographic East and down, in order to collect all the component vectors of the magnetic field. (Merrill, McElhinny & McFadden 1998, 20.)

3.2 Magnetic Hysteresis

The magnetic hysteresis loop in Figure 2 illustrates the behaviour of a ferromagnetic core as the relationship of *B* and *H* is non linear. Where *B* is the magnetic flux density for a particular material and *H* is the magnetic field strength to which the material is exposed. The magnetic field strength of *H*, to which the

material is exposed, shown on the *x*-axis, and the resulting magnetic flux density of the material *B* is plotted on the *y*-axis. (Serway 1990, 858 .)

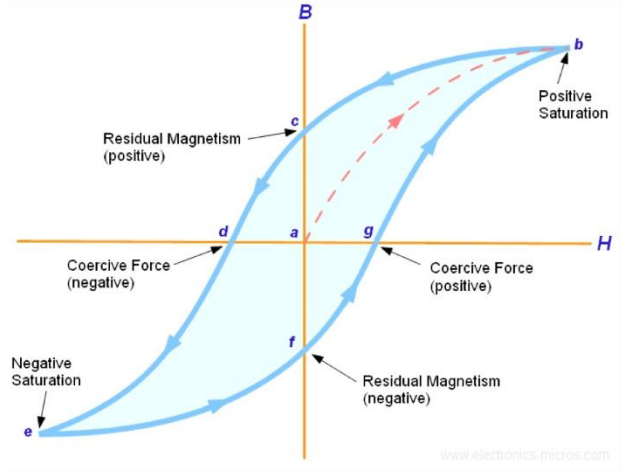

Figure 2. *B-H* Curve (Electronics & Micros 2017)

When a ferromagnetic material such as iron is tested experimentally, a hysteresis curve similar to Figure 2 is produced. There is an upper and lower limit to the magnetic flux density *B*, that can be achieved, referred to as the positive and negative saturation respectively. This is related to the crystalline structure of iron, where each crystal is a unique magnetic domain. Initially each domain has random magnetic orientation. As the magnetic field strength *H* is increased, the number of magnetic domains that align with the external magnetic field *H* also increases. When all magnetic domains have aligned themselves with the magnetic field strength *H*, no further increase in magnetic flux density *B* is possible, and the material is said to be saturated. In Figure 2 the core is saturated at point *b* in the positive cycle and point e in the negative cycle. (Serway 1990, 858.)

When the core is alternatively magnetized in positive and negative directions, magnetic hysteresis or “lag” is observed. When initially magnetized for the first time the curve follows the dashed line from point *a* to point *b*, but when *H* is reduced to zero, some residual magnetism remains. This can be seen at point *c* where *H* is zero and *B* is positive, it is known as the remnant flux density. To achieve complete demagnetization, a negative magnetic field strength *H* is

required, which can be seen at point d and is called the coercive force (negative). (Serway 1990, 858.)

As the negative cycle continues negative saturation is achieved at point *e*. When magnetic field strength *H* is reduced back to zero point *f* is reached, negative residual magnetism. Magnetic field strength *H* increases becoming more positive, the flux density *B* is reduced to zero at point *g* and is called the coercive force (positive). As *H* increases to its maximum the curve returns to point b, positive saturation. (Serway 1990, 858.)

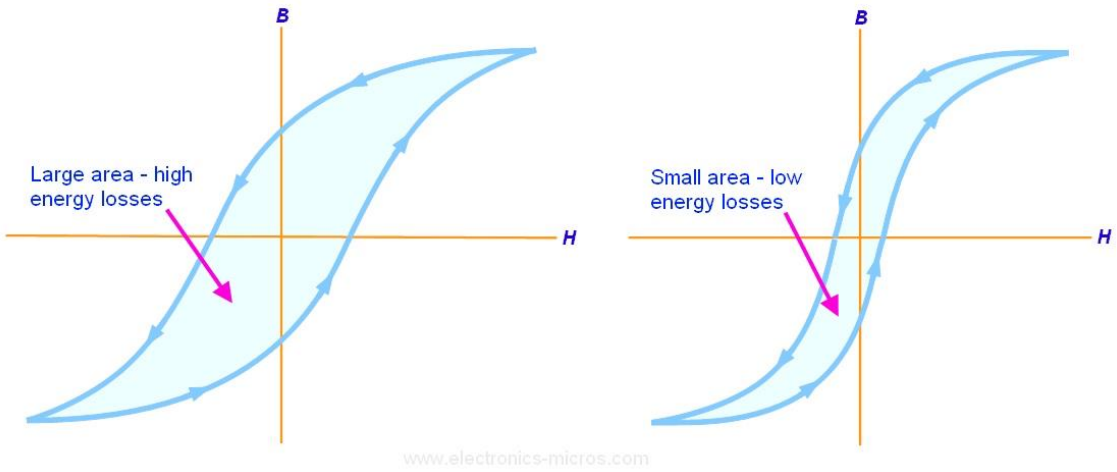

Figure 3. Hysteresis energy losses (Electronics & Micros 2017)

The area described by the *B*-*H* curve is proportional to the energy loss within the ferromagnetic material. The harder the ferromagnetic material the greater the hysteresis losses, as more energy is required to realign the magnetic domains. Soft ferromagnetic materials have higher values of relative permeability. Iron has a value for relative permeability of 5 000. Whereas mu-metal a nickel-iron alloy has a permeability of 50 000 or better. Metglas is a thin amorphous metal alloy ribbon created by a rapid solidification process, in the order of 1 000 000 degrees Celcius per second. The rapid solidification disrupts the formation of a crystalline structure and creates unique ferromagnetic properties. This allows magnetization and demagnetization to occur more rapidly than alloy with a crystalline structure.

Metglas exhibits very low core losses with a relative permeability of approximately 1 000 000. The most sensitive fluxgate sensors use Metglas for the core material. (Brauer et al. 2000, 185.)

3.3 Fluxgate Sensor

Fluxgate magnetic sensors were invented by H. Aschenbrenner and G. Goubau in 1936. Initially they were used in geological surveying to detect the magnetic alignment of rock strata. Later, during World War II they were developed by Victor Vacquier as airborne magnetometers to detect submarines. (Du 2015, 197.)

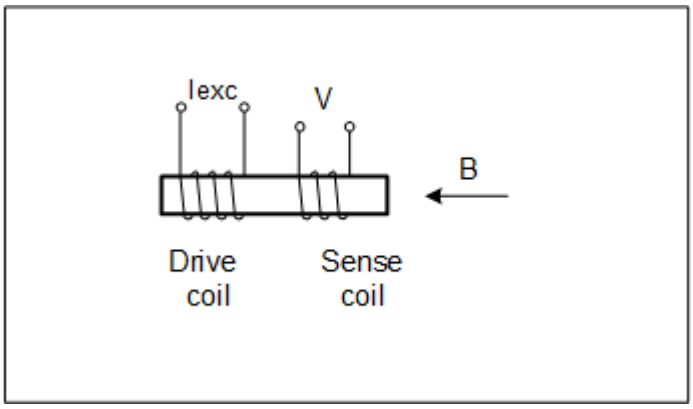

Figure 4. Fluxgate Sensor

The sensor consists of a small core of highly magnetically permeable material around which are wound a drive coil and a sense coil. The drive coil is supplied with an alternating current (Iexc) which drives the core material through alternating cycles of full magnetic saturation. This is referred to as the excitation current (Iexc). When the current is at a peak, the magnetic field of the drive coil is also at a peak value which is sufficient to fully saturate the core material with its magnetic field. Since the core is saturated, any external field has no effect on the core. The magnetic gate is closed. When the alternating current reverses the magnetic field collapse to zero as it transitions to the opposite polarity. It is during this transition that core becomes unsaturated and regains the ability to absorb the magnetic fields in the ambient surroundings. If the is no ambient magnetic field (B), then the output of the sense coil will match the frequency of the drive coil. When there is an ambient magnetic field present, static or in transition, it will

induce a voltage, V into the sense coil during the period of core unsaturation. (Bratland, Caruso, Schneider, Smith 1998, 3.)

The core of a fluxgate sensor maybe formed in different types of geometry. The fluxgate sensor on board the space satellite Astrid-2, uses a ringcore. The ringcore has a diameter of 17 mm and is formed by 11 wraps of the amorphous ribbon VITROVAC 6025 from Vacuum-schmelze, Germany. The amorphous ribbon is wound in a groove cut into a toroidal bobbin made of magnetically inert substance called MACOR. The excitation coil is wound toroidally and symetrically on the ringcore. The sense coil or detector coil as it is also known, is made to compass the excitation core and ring core. (Brauer, Risbo, Merayo & Niesen 2000, 184.)

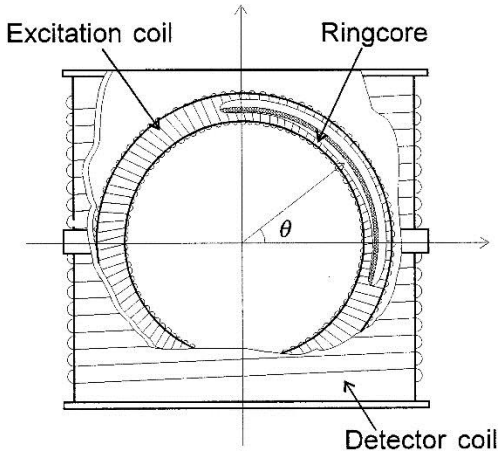

Figure 5. Toroidal Core (Brauer et al. 2000, 184)

There are several methods to detect the signal from the sense winding. The drive signal is a square wave which is composed of only odd harmonics of the fundamental frequency. Therefore if there is no external magnetic field influencing the sense coil, then only odd harmonics of the drive frequency will be present. If any even harmonics are induced into the sense coil then they must be from an external source. Phase synchronous detection is one method used to extract even harmonics and quantify to produce a scalar value. Alternatively the sense signal is conditioned through a Schmitt trigger circuit to square the rising edges, and the time period between successive rising edges measured. The change in time period is proportional to the external magnetic field. (Cerman, Kuna, Ripka & Merayo 2005, 422.)

The FGM-3 sensor used in this study, is a commercially manufactured flux-gate sensor made by Speak & Co Llanfapley, in the United Kingdom. It has power requirements of 12 mA at 5 volts DC. The output is a TTL (Transistor Transistor Logic) 5 volts PWD (Pulse Width Modulation) the time-period of which is in the range of 5 to 25 µs. Its sensitivity is ±50 000 nanoTesla. The external case dimensions are 61 mm long, 15 mm diameter. The external case has a slight taper, the sides are not parallel therefore it is not cylindrical but rather, conical in longitudinal cross section. The operating temperature range is zero to fifty degrees Celcius. (Speake & Co Llanfapley 2016.)

4 METHODS

4.1 The Vector Product

The vector product, also known as the cross product, is a method to calculate the magnitude and direction of a vector product. The vector product of $\vec{A}$ and $\vec{B}$, written $\vec{A} \times \vec{B}$, produces a third vector $\vec{C}$ whose magnitude is $|C| = |A||B| \sin\theta$. Where θ is the smaller of the two angles between $\vec{A}$ and $\vec{B}$. The smaller angle between the two vectors must be used because $\sin\theta$ and $\sin(360 - \theta)$ differ in algebraic sign. The direction of $\vec{C}$ is perpendicular to the plane defined by $\vec{A}$ and $\vec{B}$, its direction is given by the right hand rule, where the outstretched thumb points in the direction of $\vec{C}$. (Halliday, Resnick & Walker 2011, 50.)

Note that the order of vector multiplication is important. Indeed, the multiplication is anticommutative, that is

$$\vec{A} \times \vec{B} = -(\vec{B} \times \vec{A}).$$

Since the natural curve of the fingers of the right hand must be in the direction of the small angle between the two vectors. When the right hand fingers curve in from B towards A, the thumb points in the opposite direction downwards, as when the fingers curve from A towards B. (Halliday, Resnick & Walker 2011, 51.)

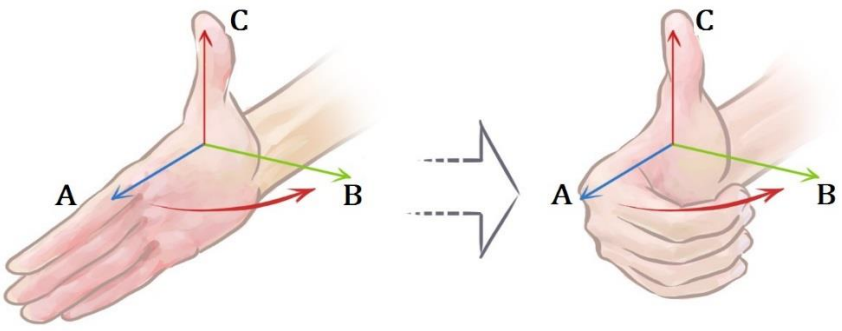

Figure 6. Vector Product Right Hand Rule (Suoto 2017)

The notation $\vec{A} \times \vec{B}$ is why the vector product is also known as the cross product and why in speech it is referred to as “A cross B.”

4.2 The Law of Biot-Savart

> Shortly after Oested´s discovery in 1819 that a compass needle is deflected by a current carrying conductor, Jean Baptiste Biot and Felix Savart reported that a conductor carrying a steady current produces a force on a magnet. From their experimental results, Biot and Savart were able to arrive at an expression that gives magnetic field at some point in space in terms of the current that produces the field. (Serway 1990, 836.)

The law of Biot-Savart states that if a wire carries a steady current I, the magnetic field $d\vec{B}$ at a point P due to a small element of wire $d\vec{s}$ as shown in Figure 7, has the following properties:

- The vector $d\vec{B}$ is perpendicular both to $d\vec{s}$, which is in the direction of the current, and to the unit vector $\hat{r}$ directed from the element to the point P.
- The magnitude of $d\vec{B}$ is inversely proportional to r^2 where r is the distance from the element $d\vec{s}$ to the point P.
- The magnitude of $d\vec{B}$ is proportional to both the current and to the length $d\vec{s}$ of the element.
- The magnitude of $d\vec{B}$ is proportional to $\sin\theta$, where θ is the angle between the vector $d\vec{s}$ and the unit vector $\hat{r}$. (Serway 1990, 836.)

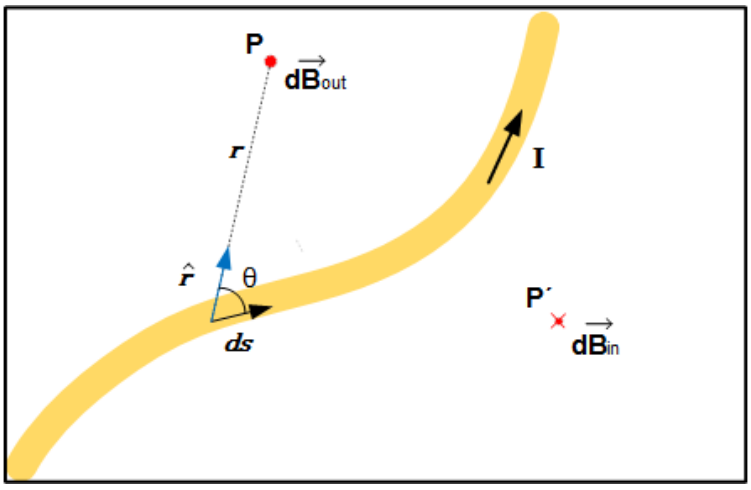

Figure 7. Magnetic Field $d\vec{B}$ Due to a Current Element $d\vec{s}$ (Serway 1990, 836)

The law of Biot-Savart can be summarized in the following form:

$$d\vec{\mathrm{B}} = k\ \frac{\mathrm{I}\, d\vec{s} \times \hat{r}}{r^2} \qquad (1)$$

Where k is a constant that in SI units is exactly 10^{-7} Wb/Am

The constant k is usually written $\frac{\mu_0}{4\pi}$ where μ_0 is another constant, called the permeability of free space. That is

$$\frac{\mu_0}{4\pi} = k = 10^{-7} \text{ Wb/Am} \qquad (2)$$

$$\mu_0 = 4\pi k = 4\pi \times 10^{-7} \text{ Wb/Am} \qquad (3)$$

Hence the law of Biot-Savart may also be written

$$d\vec{\mathrm{B}} = \frac{\mu_0 \mathrm{I}}{4\pi}\ \frac{d\vec{s} \times \hat{r}}{r^2}\ , \qquad (4)$$

where the permeability of free space replaces the constant k. (Serway 1990, 836.)

The law of Biot-Savart can be derived by considering the magnetic force caused by a single charged particle. A charged particle when moving through space creates a magnetic field. The magnetic field around the moving charged particle decreases with distance from the particle. Using the right hand rule, where the thumb points in the direction of movement, the right hand fingers point in the direction of the magnetic field around the charged particle. (Van Biezen 2014.)

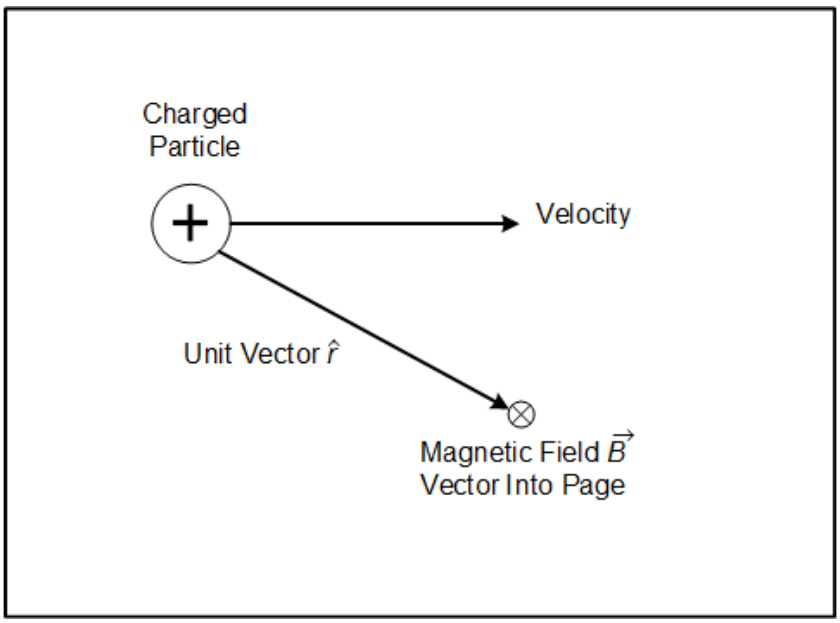

Figure 8.The Magnetic Field Around a Moving Charged Particle

The magnetic field vector $\vec{\mathrm{B}}$ caused by a single charged particle at the position shown is given by

$$\vec{\mathrm{B}} = \frac{\mu_0}{4\pi} \frac{q\,\vec{v}\times\hat{r}}{r^2} \quad , \qquad (5)$$

where

μ_0 = permativity of free space

q = charge of the particle

$\vec{v}$ = velocity of the particle

$\times$ = the cross product

$\hat{r}$ = unit vector

r = distance

The law of Biot-Savart takes the concept of magnetic force created by a charged particle and applies it to the current carried by an infinitely small segment of wire referred to as $d\vec{s}$. (Van Biezen 2014.)

The current density inside a conductor is given by

$$J = \frac{I}{A} , \qquad (6)$$

where

J = current density

I = current

A = cross sectional area

$$J = n\, q\, v_d , \qquad (7)$$

where

n = number of free charges per unit volume

q = charge on each charged particle

v_d = drift velocity of charged particles

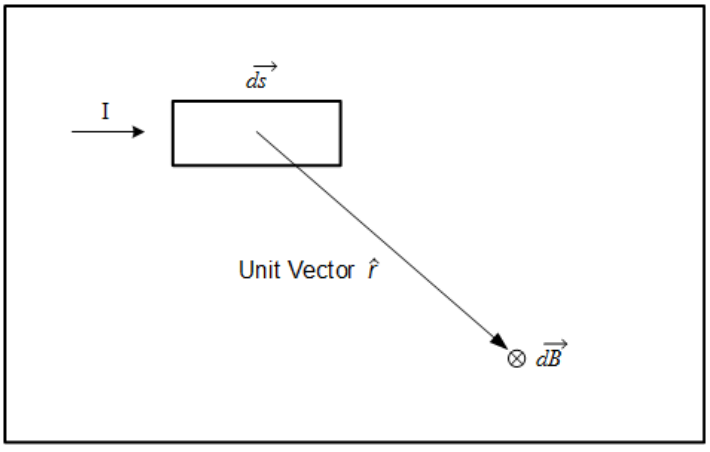

Figure 9. Segment of Wire ds, and Magnetic Field $d\vec{\mathrm{B}}$

By defining the charge in the segment ds as dQ, one obtains

$$dQ = n\, q\, dV . \qquad (8)$$

Thus, dQ equals n, the number of charged particles per unit volume, multiplied by the charge on each particle q, multiplied by the volume dV. Here dV is the product of cross sectional area and length, consequently

$$dQ = n\ q\ A\ ds\ . \qquad (9)$$

This gives the amount of charge within the small length of wire. Since ds is assumed to be infinitely small, dQ is assumed to be the same as the charge on a single particle, and therefore the same as q in Formula (5).

Now $\vec{\mathrm{B}}$ becomes $d\vec{\mathrm{B}}$ since it is a small part of the magnetic field. In conclusion,

$$d\vec{\mathrm{B}} = \frac{\mu_0}{4\pi}\ \frac{dQ\ \overrightarrow{V_d} \times \hat{r}}{r^2}\ . \qquad (10)$$

Substitution of $\mathrm{dQ} = \mathrm{n\ q\ A\ dl}$ in (10) yields

$$d\vec{\mathrm{B}} = \frac{\mu_0}{4\pi}\ \frac{n\ q\ A\ dl\ \overrightarrow{V_d} \times \hat{r}}{r^2}\ . \qquad (11)$$

From equalities (6) and (7), one obtains

$$\frac{I}{A} = n\ q\ v_d\ , \qquad (12)$$

From which

$$v_d = \frac{\mathrm{I}}{A\ n\ q}\ . \qquad (13)$$

The drift velocity is substituted to give

$$d\vec{\mathrm{B}} = \frac{\mu_0}{4\pi}\ \frac{n\ q\ A\ \mathrm{I}\ d\vec{s} \times \hat{r}}{A\ n\ q\ r^2}\ , \qquad (14)$$

which after canceling terms, gives the law of Biot-Savart

$$d\vec{\mathrm{B}} = \frac{\mu_0 \mathrm{I}}{4\pi} \frac{d\vec{s} \times \hat{r}}{r^2} . \qquad (15)$$

As has been shown, the magnetic field for a single charged particle can be calculated as in Formula (5). Therefore, the concept can be expanded to find the magnetic field created by a small current segment $d\vec{s}$ as in Formula (15). (Van Biezen 2014.)

The law of Biot-Savart gives the magnetic field at a point only for a small element of the conductor. The total magnetic field B at some point due to a conductor of finite size, requires the summation of the magnetic fields contributed from all elements that make up the conductor. Thus the summation is achieved by integrating the law of Biot-Savart as follows

$$\mathrm{B} = \frac{\mu_0 \mathrm{I}}{4\pi} \int \frac{d\vec{s} \times \hat{r}}{r^2} . \qquad (16)$$

Where the integral is taken over the entire conductor. This expression must by handled with special care since the integrand is a vector quantity. (Serway 1990, 836.)

4.3 The Magnetic Field of a Thin Straight Conductor

A thin straight wire carrying a constant current I and placed along the x axis as in Figure 10. The law of Biot-Savart can be applied calculate the total magnetic field at point P located at a distance a, from the wire.

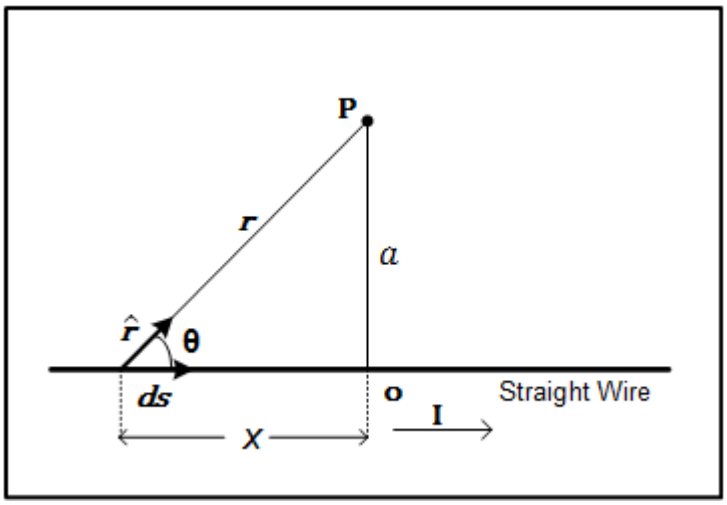

Figure 10. Magnetic Field Due to a Straight Wire (Serway 1990, 837)

An element *ds* is at a distance *r* from point P. The direction of the field at point P due to this element is out of the page, since by the right hand rule the vector product of $d\vec{s} \times \hat{r}$ is out of the page. All elements of the conductor give the same direction of magnetic field contribution, out of the page at point P.

By taking the origin at O and positioning P along the positive y axis with *k* being the unit vector pointing out of the page, we see that.

$$d\vec{s} \times \hat{r} = k|d\vec{s} \times \hat{r}| = k(dx\, sin\theta) \qquad (17)$$

Substitution into the law of Biot-Savart gives,

$$d\vec{B} = \frac{\mu_0 I}{4\pi} \frac{dx \sin\theta}{r^2} \qquad (18)$$

In order to integrate this expression, the variables θ, x, and r must be related. One approach is to express x and r in terms of θ. This can be derived as follows. From the geometry in figure 10, the following relationship is obtained:

$$r = \frac{a}{\sin\theta} = a\csc\theta \qquad (19)$$

Since,

$$\tan\theta = \frac{-a}{x} \qquad (20)$$

$$x = -a\cot\theta \qquad (21)$$

$$dx = a\csc^2\theta\, d\theta \qquad (22)$$

Substituting dx into (18) gives

$$d\vec{B} = \frac{\mu_0 I}{4\pi}\frac{a\csc^2\theta\,\sin\theta\,d\theta}{a^2\csc^2\theta} \qquad (23)$$

$$d\vec{B} = \frac{\mu_0 I}{4\pi a}\sin\theta\, d\theta \qquad (24)$$

The expression has been reduced to a single variable, θ. The total magnetic field at point P is obtained by integrating over all elements subtending angles in the range from $\theta 1$ to $\theta 2$, as shown in Figure 11. (Serway 1990, 837).

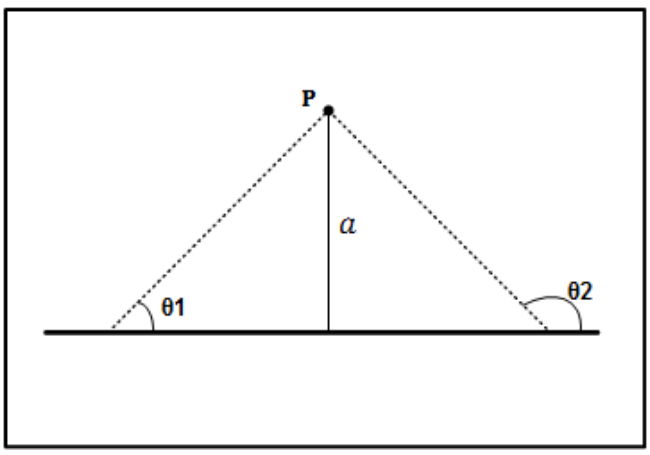

Figure 11. Limiting Angles (Serway 1990, 837)

$$\mathrm{B} = \frac{\mu_0 \mathrm{I}}{4\pi a} \int_{\theta 1}^{\theta 2} \sin d\theta = \frac{\mu_0 \mathrm{I}}{4\pi a} \left(\cos \theta 1 - \cos \theta 2 \right) \qquad (25)$$

This equation can be applied to calculate the magnetic field of any straight wire where the angles $\theta 1$ and $\theta 2$ are known. If the conductor forms one side of a square current loop, the magnetic force at the center point can be calculated using angles of 45 and 135 degrees. (Serway 1990, 838).
For one side of a square loop,

$$\mathrm{B} = \frac{\mu_0 \mathrm{I}}{4\pi a} \left(\cos 45° - \cos 135° \right) \qquad (26)$$

Since, $\cos 45° - \cos 135° = \sqrt{2}$

$$\mathrm{B} = \sqrt{2} \frac{\mu_0 \mathrm{I}}{4\pi a} \qquad (27)$$

The magnetic field at the center point of the square loop is composed of fields from all four sides in superposition. Thus, the right side of the equality, is multiplied by four as in (28). (Inan & Inan 1999, 456.)

$$\mathrm{B} = \sqrt{2} \frac{\mu_0 \mathrm{I}}{\pi a} \qquad (28)$$

For a current loop made up of several turns the sum effect of multiple loops must taken into account by multiplying equation (28) by n, where n represents the number of loops.

$$\mathrm{B} = \sqrt{2} \frac{\mu_0 \mathrm{I}}{\pi a} n \qquad (29)$$

To find a suitable value for the number of loops, calculate a value for flux density with a single loop, in equation (29) let n equal 1. Let a, equal half the length of

the side of the square current loop, 0.25 m and I equal 1.3 Amperes, the maximum for the 0.3 mm diameter copper wire.

$$\mathrm{B} = \frac{(\sqrt{2})(4\pi \times 10^{-7})(1.3)(1)}{0.25\pi}$$

The calibrating field for one turn of the current loop coil, B = 2 941 nT

The geomagnetic field in non storm conditions has a scalar value in the range of approximately 25 000 to 65 000 nT depending on location. Here at the arctic circle in Finnish Lapland the strongest component of geomagnetic field is in the vertically down *z*-axis and has a value of approximately 50 000 to 55 000 nT. Therefore it was considered that twenty turns was an appropriate number for the current loop coil to produce a field of sufficient flux density to cancel the geomagnetic field in any single axis.

In Figures 12 to 14 the direction of the resulting calibration field produced by the current loop coil is in the direction of the *x*-axis perpendicular to the current loop. The current loop can be mounted in any alignment, hence the *x*-axis in the figures can be directed in any geomagnetic axis. The magnetic fields produced in the y- and *z*-axis are in exact opposition, cancelled out by each opposite side of the square, since the current flows in opposite directions. Figure 12 illustrates how the fields in the *y* and *–y* coordinates cancel. Figure 13 illustrates how the fields in the *z* and *–z* coordinates cancel. Finally, Figure 14 illustrates the effect of superposition cancelling opposing fields exactly, since the current is equal and opposite, on opposite sides of the square. The geometry of the square current loop creates an absence of any field in the *y* and *z* coordinates. Only the the *x*-axis has a magnetic field unopposed by geometry, this calibrating magnetic field is positioned vertically upwards to oppose the geomagnetic field in the downwards direction. The geomagnetic field in the *z*-axis downwards, is cancelled by the calibrating magnetic field of the current loop coil in the vertically upwards direction. The extent to which the geomagnetic field is diminished by the calibrating magnetic field of the current loop coil, depends on the current flowing through it.

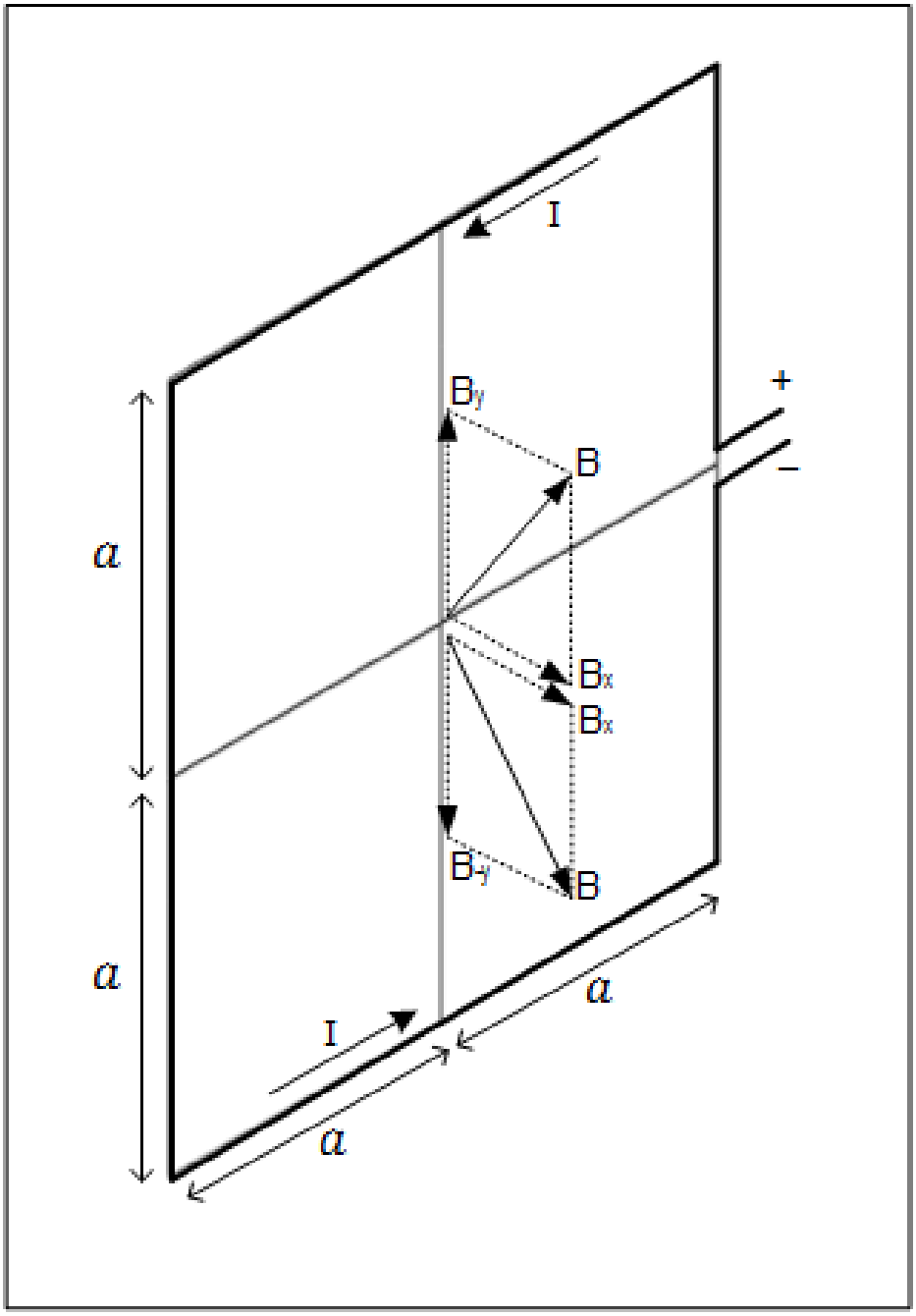

Figure 12. Y-axis Superposition

Figure 12 illustrates that the magnetic field produced by the horizontal sides of the square current loop is perpendicular to the current with components in the *x*- and *y*-axis. The upper side of the loop produces fields in the *x*- and the *–y*-axis. Whereas the lower side of the loop produces fields in the *x*- and the *y*-axis. Since both the upper and lower edge of the current loop carry the same current, the field in the *y*- and *-y*-axis cancel each other exactly, the resulting field is observed only in the *x*-axis.

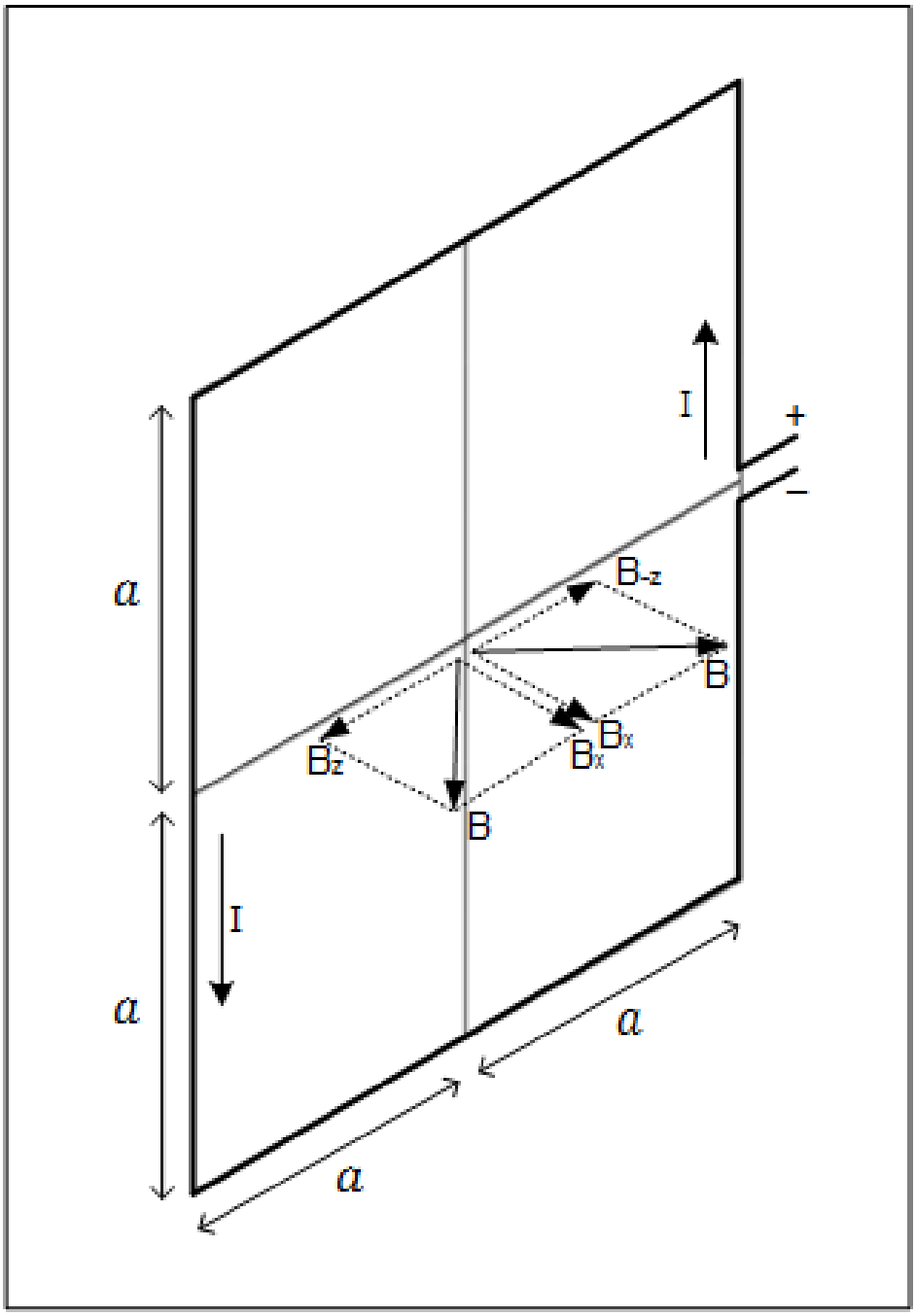

Figure 13. Z-axis Superposition

Figure 13 illustrates that the magnetic field produced by the vertical sides of the square current loop is perpendicular to the current with components in the *x* and *z*-axis. The left side of the loop produces fields in the *x*- and the -*z*-axis. Whereas the right side of the loop produces field in the *x*- and the *z*-axis. Since both the left and right edge of the current loop carry the same current, the field in the *z*- and -*z*-axis cancel each other exactly, a resulting field is observed only the in the *x*-axis.

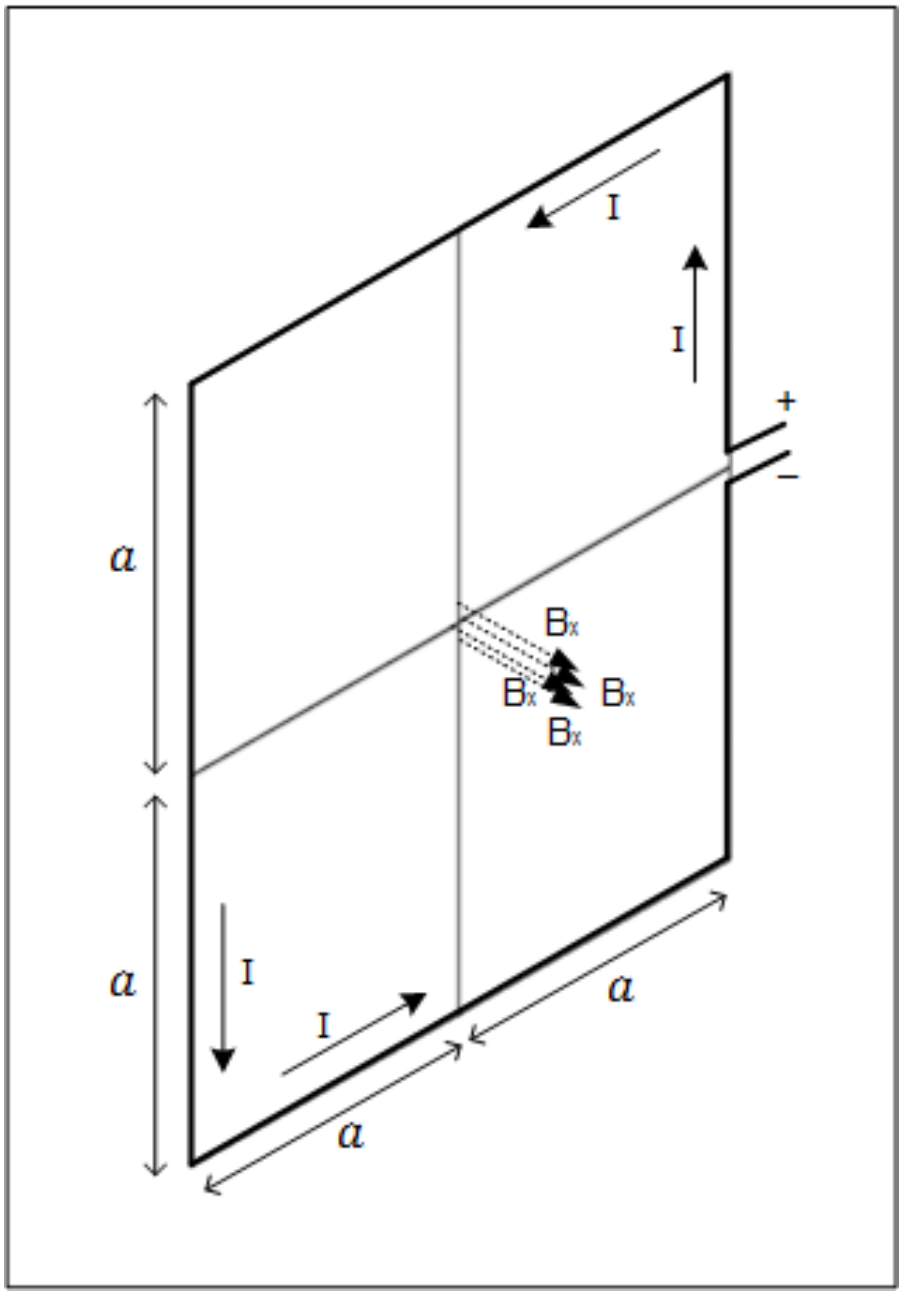

Figure 14. Square Current Loop Magnetic Field

Figure 14 illustrates the result of superposition of the magnetic fields from all four sides of the square current loop. A resultant magnetic field is produced perpendicular to the plane of the current loop, illustrated in the *x*-axis.

4.4 Fluxgate Calibration Method

The calibration was accomplished with a 500 mm square current loop comprised of 20 turns of 0.3 mm diameter enameled copper wire. The square current loop windings were made side by side on the Styrofoam armature, thus the length of the windings was less than 10 mm. In the center of the current loop a hole in the Styrofoam to allow the fluxgate sensor to be inserted. A three Amperes DC (Direct Current) power supply with digital current metering was connected to the square current loop. With the sensor in the vertical axis, pointing downwards, the current was adjusted so that the magnetic field created at the center of the square current loop cancelled the ambient geomagnetic field in the *z*-axis. The output of the FGM-3 fluxgate sensor was connected to a digital oscilloscope, where the time-period of the duty cycle was read. A diagram of the fluxgate sensor calibration apparatus is illustrated in Figure 16.

A value for the *z*-axis geomagnetic field was obtained by referring to online real-time data from the web site of Sodankylä Geophysical Observatory. At the time of the tests the value for geomagnetic field in the *z*-axis was 51 655 nT. Using the law of Biot-Savart with a known current flowing through the square current loop, the resultant magnetic field B produced at the center of the current loop was calculated using Equation (29).

$$\mathrm{B} = \sqrt{2}\frac{\mu_0 \mathrm{I}}{\pi a} n$$

The current loop was positioned in the horizontal plane, with the direction of the current flow such that the magnetic field B opposed the geomagnetic field in the vertical *z*-axis. The resultant magnitude of magnetic field strength that the fluxgate sensor experienced was equal to the *z*-axis geomagnetic component of 51 655 nT minus the value of B created by the calibrating current flowing through the square current loop.

The calibration method created a magnetic field that reduced the geomagnetic *z*-axis field to less than zero with a calibrating current of 1.2 Amperes. The diameter of the enameled copper wire was the limiting factor in the maximum current used.

By reducing the calibration current successively a range of results from zero to full geomagnetic field in the *z*-axis was achieved. By plotting the results, the linearity of the sensor was observed.

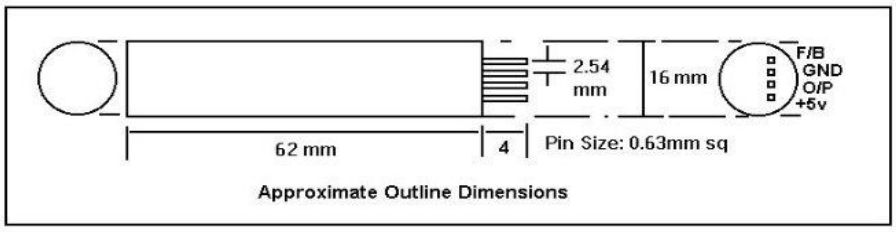

Figure 15. FGM-3 Fluxgate Pin Diagram (Speake & Co Llanfapley, 2016)

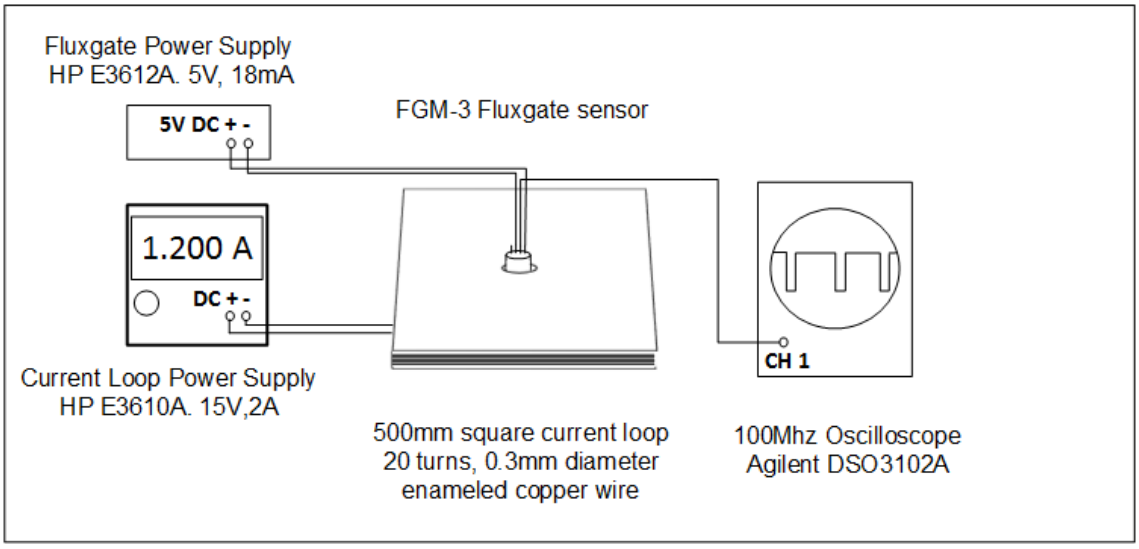

Figure 16. Fluxgate Calibration Apparatus Diagram

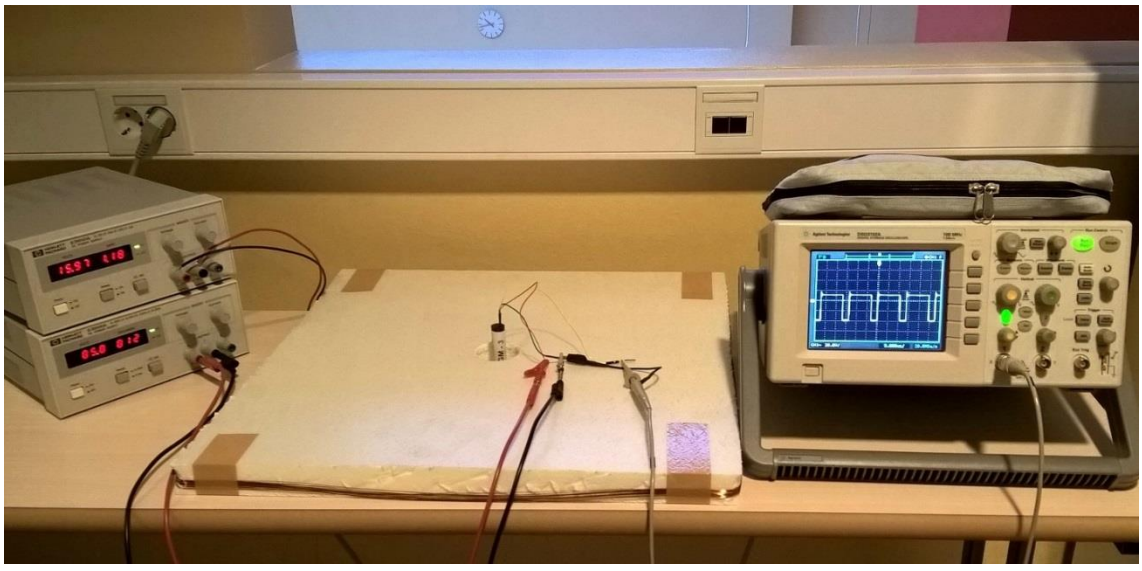

Figure 17. Fluxgate Square Current Loop Calibration Apparatus

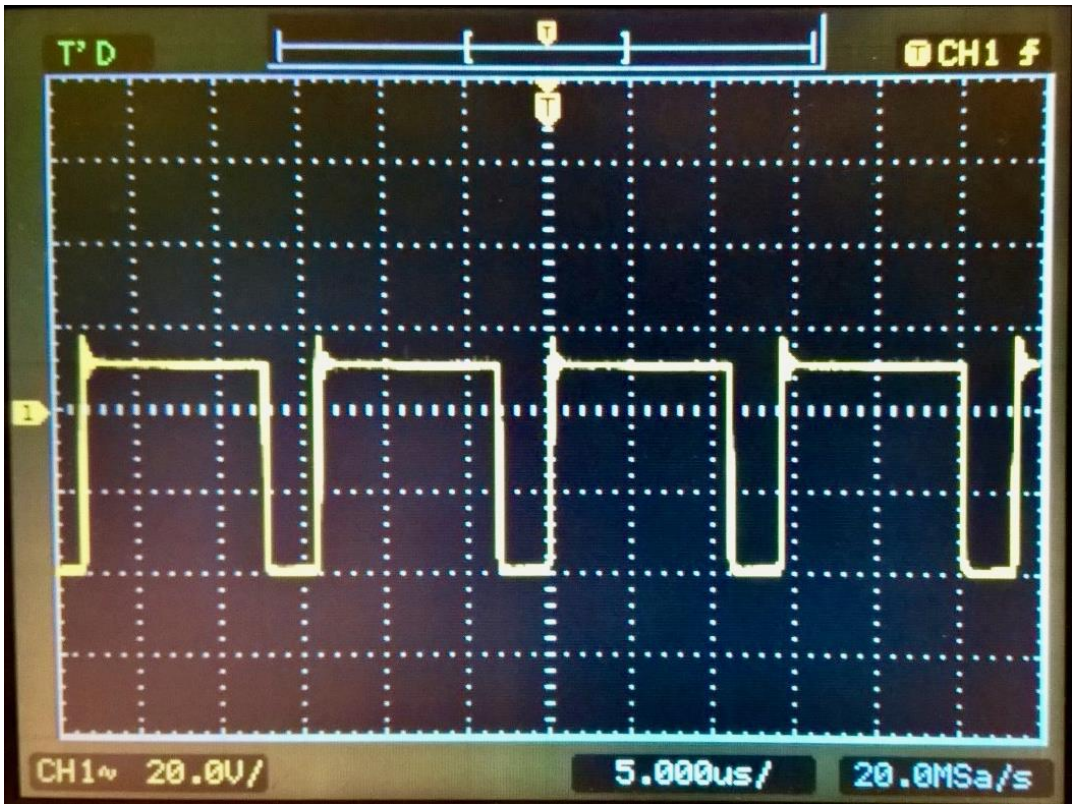

Figure 18. Fluxgate Output Signal Time Period 14 µs

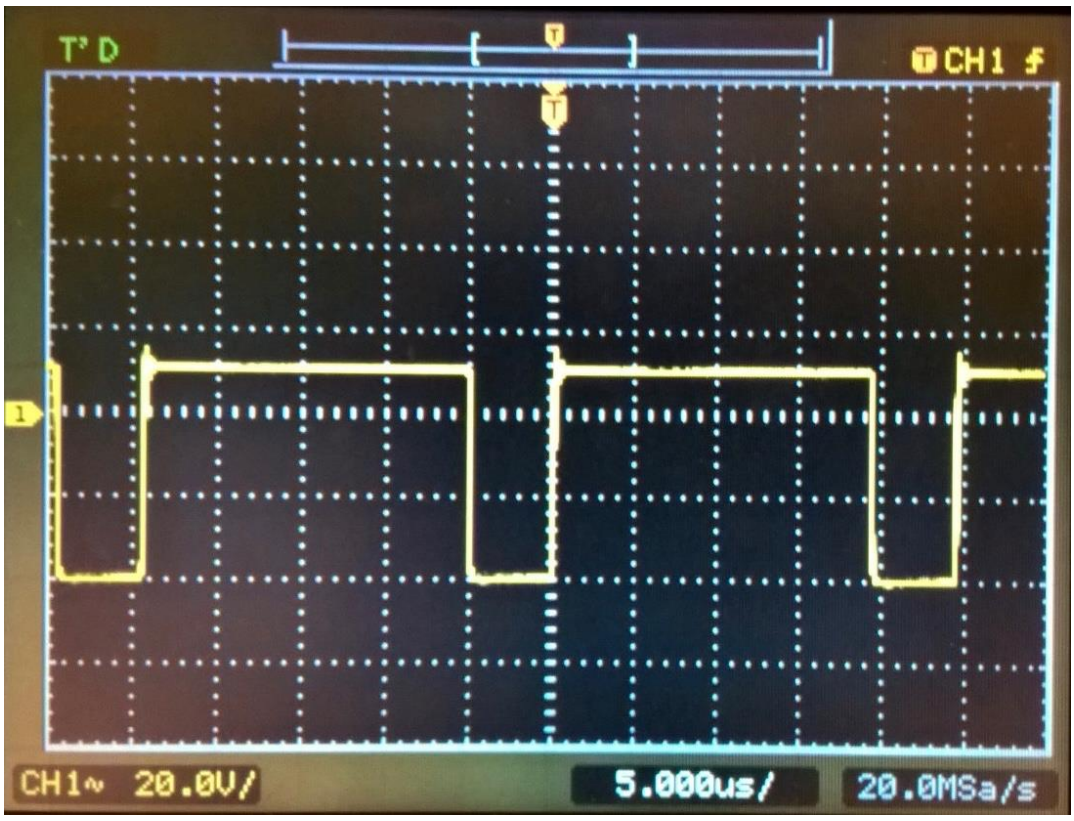

Figure 19. Fluxgate Output Signal Time Period 24 µs

5 RESULTS

5.1 Calibration Results

Table 1. Sensor Response to Square Current Loop

Current (A)	loop field (nT)	Geomagnetic z-axis – loop field (nT)	Fluxgate sensor output time-period (µs)
0.0	0.0	51 655	25.0
0.1	4 525	47 131	24.0
0.2	9 051	42 605	23.5
0.3	13 576	38 079	22.5
0.4	18 102	33 553	22.0
0.5	22 627	29 028	21.0
0.6	27 153	23 902	20.0
0.7	31 678	19 977	19.0
0.8	36 204	15 451	18.0
0.9	40 729	10 926	17.0
1.0	45 255	6 400	16.0
1.1	49 780	1 875	15.0
1.2	54 306	-2 651	14.0
1.3	58 831	-7 176	13.0

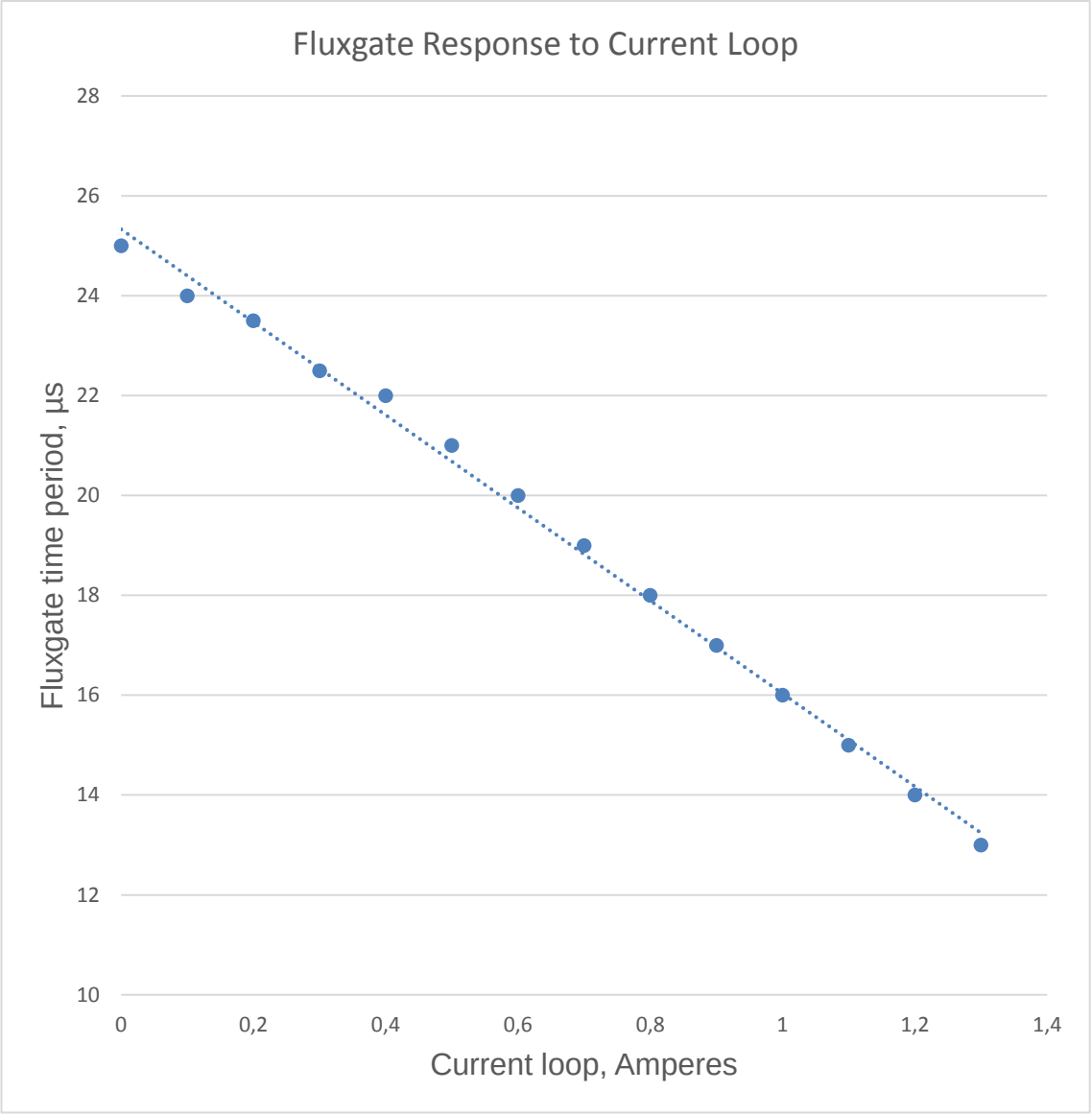

Figure 20. Fluxgate Response to Current Loop

The square current loop was positioned in the horizontal plane, the current direction produced a magnetic field upwards in the vertical plane opposing the geomagnetic field in the *z*-axis. The laboratory at LAPINAMK Rovaniemi is located at a latitude of 66 degrees North consequently the strongest component of the geomagnetic field is in the *z*-axis, down into the earth. The online website of Sodankylä Geophysical Observatory provided values for geomagnetic field strength in real-time at the time of calibration, in the *x*-axis 11 270 nT, *y*-axis 23 300 nT and *z*-axis 51 655 nT (Sodankylä Geophysical Observatory 2016).

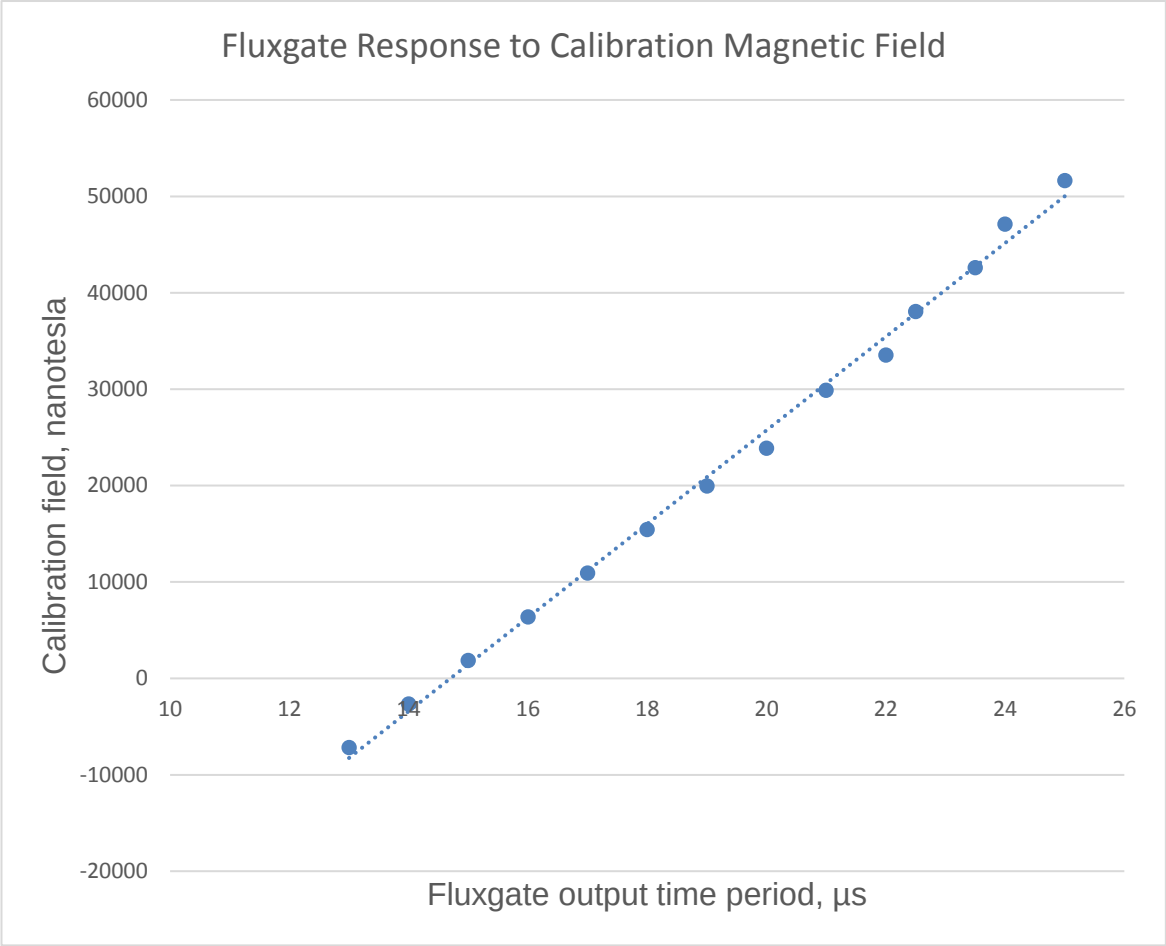

Figure 21. Fluxgate Response to Calibration Magnetic Field

Attempts at calibrating the fluxgate sensor in the *x*- and *y*-axis were unsuccessful, since it was not possible to achieve a stable output reading. The reason for constant variation was due to the simple hand held equipment not being capable of holding the sensor stable in North-South and East-West alignment. In the absence of a rigid chassis to hold the fluxgate sensor in true and steady alignment, unstable, fluctuating readings were observed on the oscilloscope. The high sensitivity and responsiveness of the sensor combined with the nature of the geomagnetic field at the Arctic circle, made small changes in orientation result in a large relative change in output signal.

Alignment with geographic North-South and East-West directions were difficult in the absence of gyroscopic surveying equipment. Surveying equipment using GPS (Global Positioning System) is unable to receive satellite signal indoors. Magnetic north alignment was attempted with a magnetic compass, but the modern building construction of the laboratory with steel water pipes overhead,

reinforced concrete floors and walls interfered with the geomagnetism considerably. It soon became apparent why magnetometer sensors at professional geophysical observatories are housed in wooden buildings that contain no metal components. In the absence of an ideal laboratory with no ferromagnetic interference and a precision mechanism to align the sensor, the calibration of the fluxgate sensor in North-South and East-West alignments were abandoned. The *z*-axis alignment vertically downwards was the only axis that was practicable to take stable fluxgate sensor readings within the laboratory environment.

6 CONCLUSIONS

The law of Biot-Savart proved to be a reliable method to calculate the magnetic field created by a current loop. The symmetry of the square current loop geometry created a magnetic field at its center, in a predetermined direction. The magnitude of the resulting magnetic field at the center of the square current loop, determined by the direct current flowing, the number of turns of wire in the coil, and the geometry of the armature, proved to be accurately predictable by the law of Biot-Savart. The method allows the magnitude of the magnetic flux density to be varied in direct proportion to the current and thus the linearity of the sensor to be observed.

7 DISCUSSION

The problems experienced with this particular laboratory method highlighted serious practical problems with the apparatus used. The magnetic environment was less than ideal with ferrous material contained within the structure of the laboratory building causing distortion of the geomagnetic field. The field for magnetic north was deflected by several degrees in most locations in the laboratory. A position in an open area outside the laboratory was selected as the most magnetically undisturbed spot on the whole floor of the building.

The sensitivity of the fluxgate sensor was such that small variations in alignment resulted in large variations in the output signal. The absence of a rigid chassis to mount the sensor presented serious challenges in reading the output on an oscilloscope screen. It was this criteria that dictated that only measurements in the *z*-axis would be taken since any small deviation in the sensor alignment made no noticeable difference in the magnetic field sensed. It became apparent that any serious attempt to measure the geomagnetic filed in North-South and East-West alignments would require gyroscopic surveying equipment, to accurately align the flux-gate sensor.

The time taken to manually read the fluxgate sensor output time-period from the oscilloscope screen limited the apparatus, only static magnetic flux densities were measurable. To take readings of a varying magnetic flux density would require a system redesign. A digital system comprised of synchronous counters driven by a clock speed of 1 MHz or higher could read the output time-period automatically. The clock start/stop function triggered by the rising and falling edges of the time period signal, would give a near instantaneous output reading. The digital system would enable the fluxgate sensor to sample varying magnetic flux density. Professional geomagnetic observatories currently measure magnetic flux density at a sampling rate of 40 Hz. To log the readings at 40 Hz would require a data logging system interfaced to the synchronous counters to record and graph the stream of output values.

Although the laboratory apparatus used was not suitable for measuring varying magnetic flux density, the system worked very well for the static flux density of the Earth´s *z*-axis magnetic field. The apparatus utilized a square current loop with a breadth of 50 cm and a length of 1 cm, which produced a focused and stable magnetic field. Modern digital power supplies with current stabilization ensured the stability of the resultant calibration magnetic field. By constructing the coil with copper wire of 0.3 mm diameter, it was possible to apply a range of currents and achieve a range of output values sufficient to plot the linearity of the fluxgate sensor from zero magnetic flux density to full geomagnetic flux density. Therefore it has been demonstrated that the law of Biot-Savart can be applied to a practical method to calibrate a fluxgate magnetometer.

.

BIBLIOGRAPHY

Bratland, T,. Carusso, M.J., Schneider, R. & Smith, C.H. 1998. A New Perspective on Magnetic Field Sensing. Accessed 10 April 2016 http://www51.honeywell.com/aero/common/documents/myaerospacecatalog-documents/Defense_Brochuresdocuments/Magnetic__Literature_Technical_Article-documents/A_New_Perspective_on_Magnetic_Field_Sensing.pdf.

Brauer, P., Risbo, T., Merayo, J.M., & Nielsen, O.V. 2000. Fluxgate sensor for the vector magnetometer onboard the ”Astrid-2” satellite. Sensors and Actuators 81, 184-188.

Cerman, A., Kuna, A., Ripka, P., & Merayo, J.M., 2005. Digitization of highly precise fluxgate magnetometers. Sensors and Actuators A 121, 421-429.

Du, W.Y., 2015. Resistive, Capacitive, Inductive, and Magnetic Sensor Technologies. Boca Raton: Taylor & Francis Group.

Electronics & Micros. B-H Curve. Accessed 23 March 2017 http://www.electronics-micros.com/electrical/b-h-curve/.

Inan, U.S., & Inan, A.S., 1999. Engineering Electromagnetics. Menlo Park: Addison Wesley Longman.

McPherron, R.L., Magentic Pulations: Their Sources and Relation to Solar Wind and Geomagnetic Activity. Accessed 28 March 2016 http://www.whoi.edu/science/AOPE/emworkshop/pdf/mcpherron.pdf.

Merrill, R. T., McElhinny, M.W. & McFadden, P. L. 1998. The Magnetic Field Of The Earth, Volume 63: Paleomagnetism , the Core, and the Deep Mantle (International Geophysics). San Diego: Academic Press.

Halliday, Resnick, & Walker, J. 2011. Principles of Physics Ninth Edition International Student Version. Hoboken: John Wiley & Sons.

Serway, R.A. 1990. Physics for Scientists & Engineers with Modern Physics, 3rd edition. Orlando: Holt, Rinehart and Winston Inc.

Sodankylä Geophysical Observatory (SGO). Accessed 19 December 2016 http://sgo.fi/Data/Magnetometer/latestMagnetometer.php.

Speake & Co Llanfapley (SCL). FGM-3 Magnetic Field Sensors. Accessed 3 October 2016 http://www.speakesensors.com/products.html.

Suoto, N. 2017. Video Game Physics Tutorial – Part 1: An Introduction to Rigid Body Dynamics. Accessed 24 February 2017 https://www.toptal.com/game/video-game-physics-part-i-an-introduction-to-rigid-body-dynamics.

van Biezen, M. 2014. Physics – E&M: Magn Field Generated by Moving Charges & Current (13 of 28) Biot & Savart Law. Accessed 19 December 2016 https://www.youtube.com/watch?v=_CE1HEbkBec.